A constitutive model for cracking of concrete based on the incremental theory of plasticity*

E. Oñate, S. Oller†, J. Oliver and J. Lubliner‡
ETS Ingenieros de Caminos, Canales y Puertos, Universidad Politécnica de Cataluña, Jordi Girona Salgado 31, 08034 Barcelona, Spain

ABSTRACT

A constitutive model based on classical plasticity theory for non-linear analysis of concrete structures using finite elements is presented. The model uses the typical parameters of non-associated plasticity theory for frictional materials and a modified Mohr–Coulomb yield surface is suggested. Onset and amount of cracking at a point are controlled by the values of the effective plastic strain and thus it can be studied by *a posteriori* postprocessing of numerical results. The accuracy and objectivity of the model is checked out with some examples of application.

INTRODUCTION

Classical models for non-linear analysis of concrete assume elasto-plastic/viscoplastic constitutive equations for compression behaviour, whereas a conceptually more simple elasto-brittle model is used for defining onset and progression of cracks at points in tension. Different versions of this model have been successfully used by Bazant and Oh[1], Glemberg[2], De Borst and Vermeer[3], Nauta *et al.*[4], and De Borst[5], for non-linear analysis of plain and reinforced concrete structures.

The elasto-brittle model, in spite of its popularity, presents various controversial features such as the need for defining uncoupled behaviour along each principal stress (or strain) direction; the use of a shear retention factor to ensure some shear resistance along the crack; the lack of equilibrium at the cracking point when more than one crack is formed; the difficulties in defining stress paths following the opening and closing of cracks under cycling loading conditions and the difficulty in dealing with the combined effect of cracking and plasticity at the damaged point.

It is well known that microcracking in concrete takes place at low load levels due to either unbonding between aggregate and mortar, or microcracking in the mortar area. Progression of cracking follows a non-homogeneous path which combines these two mechanisms together with growth and linkage of microcracks along different directions (see *Figure 1*). Experiments performed with mortar specimens[9] have shown that the distribution of microcracks follows discontinuous patterns with random orientations. This fact is supported by many researchers[6–11] who agree that microcracking at the microscopic level can be regarded as a non-directional phenomenon and that the propagation of microcracks at the aggregate level follows an erratic path governed by the random distribution of the aggregate particles. Dominant directions of cracking can be distinguished at a macroscopic level simply by following the trajectories of the damaged points (see *Figure 2*).

These facts support the idea that the non-linear behaviour of concrete can be modelled using the unified framework of the incremental theory of plasticity with an appropriate yield function to account for different tension and compression response. Cracking can then be simply interpreted as an internal damage effect which is unambiguously

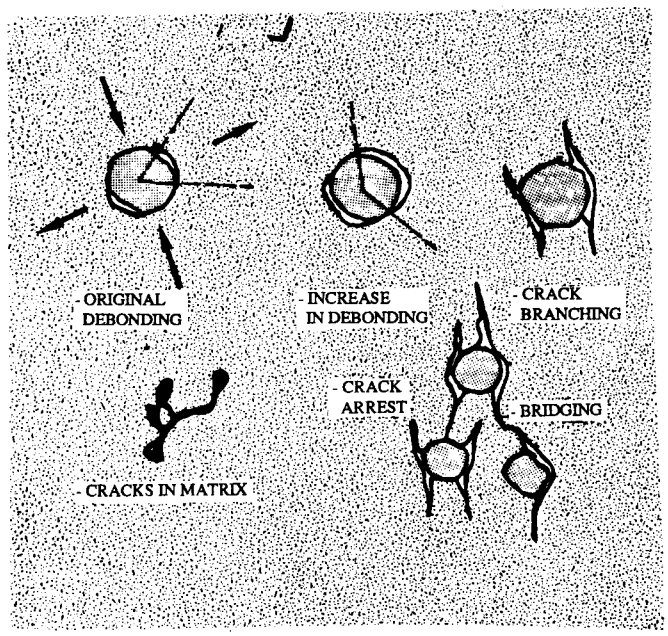

Figure 1 Mechanisms of damage[11]

* Presented at the International Conference on Computational Plasticity—Models, Software and Applications, held in Barcelona, Spain, April 1987.
† Presently on leave from: Universidad Nacional de Salta, Argentina.
‡ Present address: University of California, Berkeley, USA.

0264–4401/88/040309–11$2.00
© 1988 Pineridge Press Ltd

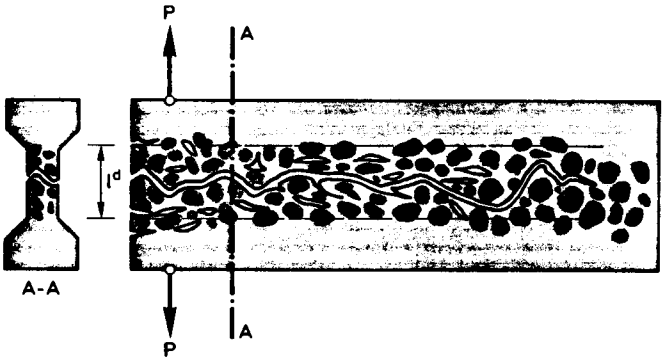

Figure 2 Propagation of cracks

monitored by well-defined parameters, such as the amount of plastic strain and the evolution (hardening/softening) of a single yield function controlling the onset and evolution of damage. Indeed, one of the main advantages of this approach is the independence of the analysis from any 'crack directions' which can be simply identified *a posteriori* once the non-linear solution has converged. This overcomes most of the problems of the elasto-brittle models mentioned earlier, and in particular the need for a discrete treatment of cracks and all the detailed stress–strain transformations at each cracked point during the solution stage.

In this paper a fully elasto-plastic model for the non-linear analysis of concrete based in the above concepts is presented. The model uses a modified Mohr–Coulomb yield surface and it includes all the important features that need to be taken into account in the non-linear analysis of concrete, such as the different response under tension or compression states, the effect of stiffness degradation, and the treatment of mesh objectivity based on the concept of specific fracture energy. The model presented here can be considered a particular class of a more general 'plastic damage' model which is currently being investigated by the authors[19,20].

The layout of the paper is the following. In the next section the main features characterizing the incremental constitutive equations are described and a modified Mohr–Coulomb yield surface is presented. The three following sections deal with the definition of the crushing function, the degradation of the elastic stiffness, and the problem of mesh objectivity, respectively. The subsequent section describes the *a posteriori* determination of cracking. Finally, some examples of application are given in the last section.

STRESS–STRAIN INCREMENTAL RELATIONSHIP: YIELD AND POTENTIAL FUNCTIONS

It is assumed that the incremental relationship between stresses and strains for both compression and tension states is obtained from classical plasticity theory[16], as:

$$d\boldsymbol{\sigma} = \mathbf{D}^{ep} \cdot d\boldsymbol{\varepsilon} \tag{1}$$

where $\mathbf{D}^{ep}$ is the standard elasto-plastic tangent stiffness matrix which for non-associated plasticity is given by:

$$\mathbf{D}^{ep} = \mathbf{D} - \frac{\mathbf{D} \cdot \left\{\frac{\partial G}{\partial \boldsymbol{\sigma}}\right\}^{T} \cdot \left\{\frac{\partial F}{\partial \boldsymbol{\sigma}}\right\} \cdot \mathbf{D}}{A + \left\{\frac{\partial F}{\partial \boldsymbol{\sigma}}\right\}^{T} \cdot \mathbf{D} \cdot \left\{\frac{\partial G}{\partial \boldsymbol{\sigma}}\right\}} \tag{2}$$

where $\mathbf{D}$ is the stiffness matrix for linear elasticity, F and G are the yield and plastic potential functions, respectively and A is the hardening parameter.

Definition of the yield function

One of the disadvantages of using the classical Mohr–Coulomb yield function for concrete is the excessive internal friction angle ϕ associated with the standard ratios of the tension and compression stresses. *Figure 3* shows that for a typical value of $R = \left|\frac{(\bar{\sigma}_{max})_{COMP}}{(\bar{\sigma}_{max})_{TEN}}\right| \cong 10$ the value of ϕ is $\simeq 60°$. This value is considerably higher than the usual dilatancy angle for concrete ($\Psi = 15°$) which explains the general need for non-associated plasticity theory (see *Figure 4*).

Traditional models use a modified version of Mohr–Coulomb yield-surface based on a simple tension cut-off[8]. This approach, however, has some of the same disadvantages as associated plasticity.

In this work a modified Mohr–Coulomb yield surface is proposed, and this is shown in *Figure 5*. The new yield surface is monitored by a reduction parameter α which allows the R–ϕ curve to be shifted towards a region in which lower values of ϕ are obtained for $R \cong 10$. Thus, it is shown in *Figure 3* that $\alpha = 1$ corresponds to the classical Mohr–Coulomb relationship and for $3.61 \leqslant \alpha \leqslant 2.16$ a value of $25° \leqslant \phi \leqslant 35°$ is obtained for stress ratios of the order of $R \cong 10$. This, indeed, alleviates the need for non-associated plasticity theory. The authors have also investigated the possibility of obtaining similar types of yield expressions for frictional materials[19,20]. It is interesting to note that

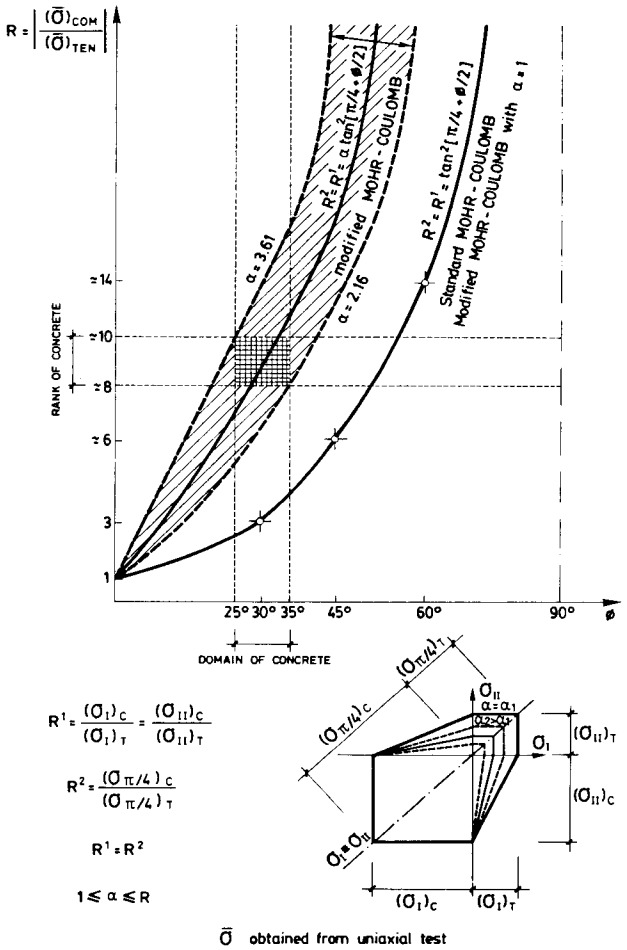

Figure 3 R–ϕ ratios for Mohr–Coulomb and modified Mohr–Coulomb surface

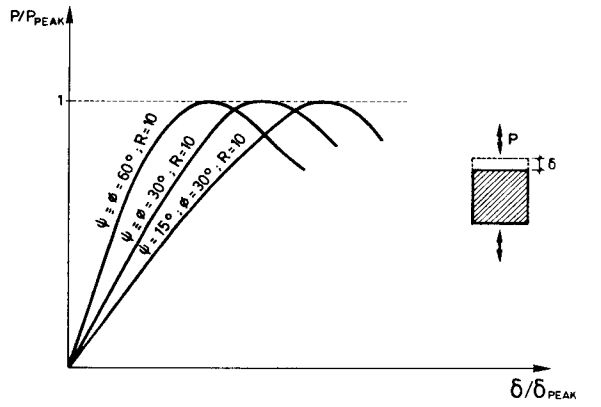

Figure 4 Schematic results for simple tension–compression test using associated and non-associated plasticity theory

for the Drucker–Prager yield function, the asymptotic character of the R–ϕ relationship (see *Figure 6*) hinders its use for practical computation.

Cohesion and internal friction angle functions

Hardening and/or softening of the yield surface is controlled by the changes in the average intergranular cohesion. *Figure 7* shows typical cohesion function in terms of the effective plastic strain for tension and compression tests. On the other hand, a constant value for the internal friction angle $\phi = 30°$ has been assumed. However, any variation of ϕ in terms of the effective plastic strain from zero to a maximum value, as typical in low cohesive materials, could be used (see *Figure 8*).

The cohesion curves control the evolution (hardening/softening) of the yield surface. Thus, the onset of plasticity (i.e. microcracking) at a point corresponds to stress values for which $F = 0$ with $c = c_{max}$ and $\phi = \phi_0$. This defines a lower limit of the yield function $F = F^I = 0$ (see *Figure 9*). As damage (cracking) progresses the yield surface changes accordingly with the updated values of the cohesion functions of *Figure 7*. This causes expansion (hardening) or contraction (softening) of the compression and tension zones, as schematically shown in *Figure 9*. The changes of the yield surface in the transition 'tension–compression' region are unambiguously monitored by defining a single

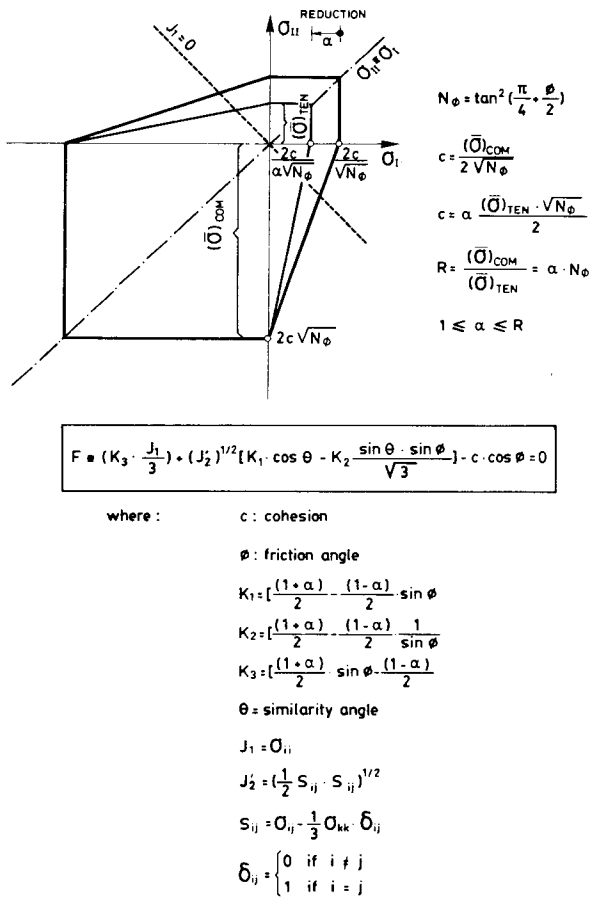

Figure 5 Modified Mohr–Coulomb yield surface

equivalent cohesion function in the following manner:

$$\frac{dc}{d\bar{\varepsilon}^p} = \beta_c(\boldsymbol{\sigma}) \cdot \frac{dc^{COM}}{d\bar{\varepsilon}^p} + \beta_T(\boldsymbol{\sigma}) \cdot \frac{dc^{TEN}}{d\bar{\varepsilon}^p} \qquad (3)$$

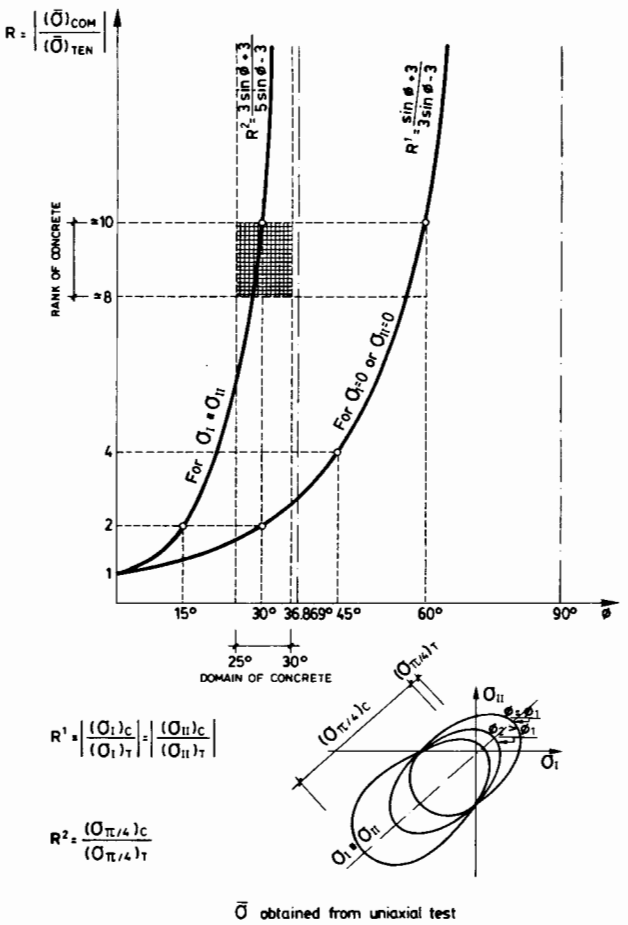

Figure 6 R–ϕ ratios for Drucker–Prager surface

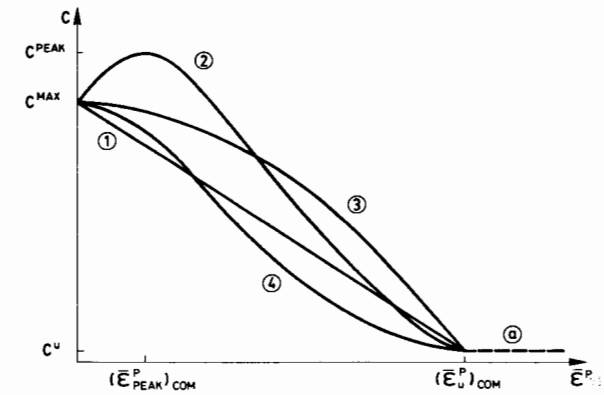

CURVES:

① ; ④ Usual for : CONCRETE UNDER TENSION [4]

③ Usual for : MASONRY UNDER TENSION AND COMPRESSION [14]

② Usual for : MOST FRICTIONAL MATERIAL UNDER COMPRESSION [3]

ⓐ CONTROLLS THE MATERIAL BEHAVIOUR BEYOND FAILURE

Figure 7 Cohesion functions

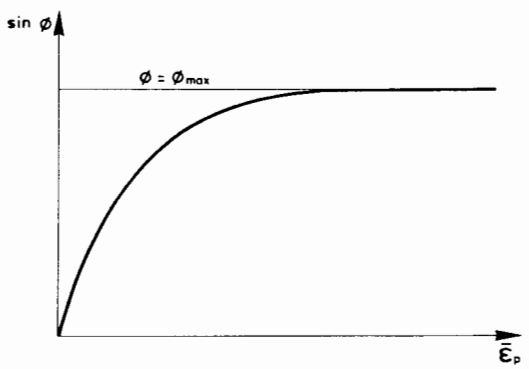

Figure 8 Friction angle function

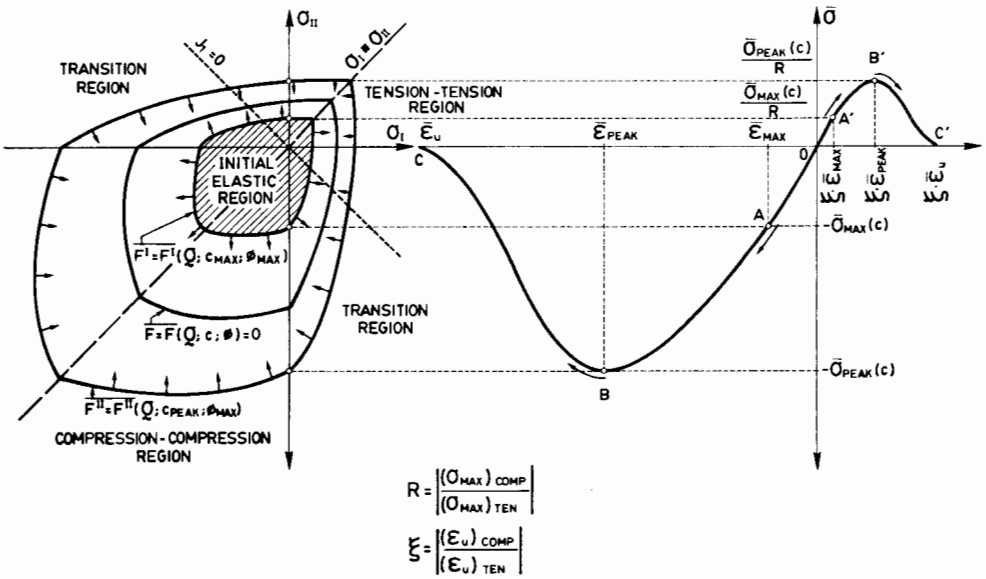

Figure 9 Schematic evolution of yield function

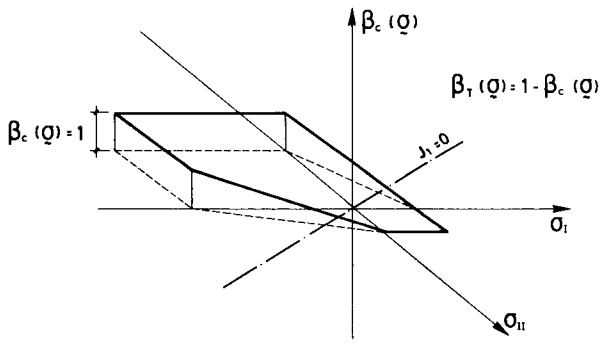

Figure 10 Weighting function β_c

with:

$$c=\int_0^{\bar{\varepsilon}^p}\frac{dc}{d\bar{\varepsilon}^p}\cdot d\bar{\varepsilon}^p$$

where c^{COM} and c^{TEN} are the cohesion function for compression and tension states, respectively, chosen from *Figure 7* and β_c and β_T are appropriate weighting functions satisfying:

$$\beta_c(\boldsymbol{\sigma})+\beta_T(\boldsymbol{\sigma})=1 \tag{4}$$

In our model we have chosen:

$$\beta_c(\boldsymbol{\sigma})=\frac{\sum_{i=1}^{3}\langle-\sigma_i\rangle}{\sum_{j=1}^{3}|\sigma_j|} \tag{5}$$

$$\beta_T(\boldsymbol{\sigma})=\frac{\sum_{i=1}^{3}\langle\sigma_i\rangle}{\sum_{j=1}^{3}|\sigma_j|} \tag{6}$$

where $\langle -x\rangle$ and $\langle x\rangle$ are the Macauley functions:

$$\langle -x\rangle=\tfrac{1}{2}(-x+|x|),\qquad \langle x\rangle=\tfrac{1}{2}(x+|x|)$$

σ_i being the principal stress in the ith direction. The form of β_c in the σ_I–σ_{II} space is shown in *Figure 10*.

Evolution of the yield function F^I progresses up to an upper limit $F^I=F^{II}=0$ (see *Figure 9*) for which $c=c_{peak}$ and $\phi=\phi_{max}$. The surface $F^{II}=0$ indicates the onset of softening under compression and the appearance of macrocracks[4,9]. For further loading the yield surface reduces its size due to global softening until the limit of damage to be accumulated at a point is reached. This is controlled by a *collapse* or *crushing* surface defined by:

$$F_c=\left[\int_{t_0}^{t_1}[d\bar{\varepsilon}^p]\cdot dt\right]-(\bar{\varepsilon}_u^p)_{COMP}=0 \tag{7}$$

where $d\bar{\varepsilon}^p$ is obtained from:

$$d\bar{\varepsilon}^p=\sqrt{\gamma\cdot\left[\left(\frac{d\varepsilon_p^I}{\xi_1}\right)^2+\left(\frac{d\varepsilon_p^{II}}{\xi_2}\right)^2\right]};\qquad \tfrac{2}{3}\leqslant\gamma\leqslant 1 \tag{8}$$

ξ_1 and ξ_2 being appropriate weights for taking into account the non-symmetry of function F_c as shown in *Figure 11*.

Potential function: dilatancy

As previously mentioned, the behaviour of granular materials can be improved by using a non-associated flow rule. In our model this is characterized by a potential function defined identically to our modified Mohr–Coulomb yield surface but using a more realistic angle of dilatancy ψ instead of the internal friction angle ϕ. The following expression for granular materials, proposed by Rowe[17], has been used

$$\psi=\arcsin\left[\frac{\sin\phi-\sin\phi_{cv}}{1-\sin\phi\cdot\sin\phi_{cv}}\right] \tag{9}$$

with:

$$\sin\phi_{cv}=\frac{\sin\phi_{max}-\sin\psi_{max}}{1-\sin\phi_{max}\cdot\sin\psi_{max}} \tag{10}$$

Typical values of ψ for concrete are $8°\leqslant\psi\leqslant 15°$.

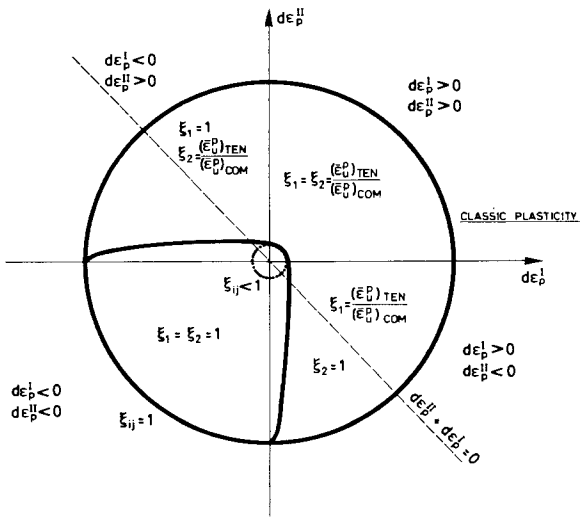

Equivalent plastic strain or Effective generalised strain :

$$d\bar{\varepsilon}_p=\sqrt{\gamma\left[\left(\frac{d\varepsilon_p^I}{\xi_1}\right)^2+\left(\frac{d\varepsilon_p^{II}}{\xi_2}\right)^2\right]};\quad \tfrac{2}{3}\leqslant\gamma\leqslant 1$$

$$\xi_i=\tfrac{1}{2}(\bar{\xi}-1)[\mathrm{SIGN}(d\varepsilon_p^i)+1]+1$$

$$\bar{\xi}=(\bar{\varepsilon}_u^p)_{TEN}/(\bar{\varepsilon}_u^p)_{COM}$$

$$F_c=\left[\int_t d\bar{\varepsilon}_p\right]-(\bar{\varepsilon}_u^p)_{COM}$$

Figure 11 Crushing function F_c

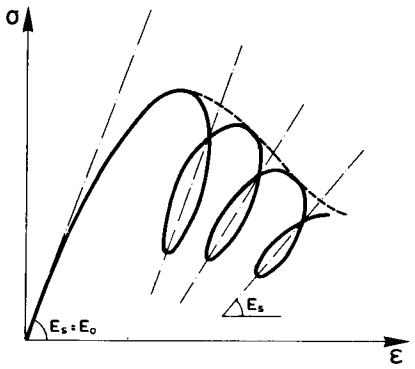

Figure 12 Degradation of secant modulus

DEGRADATION OF THE SECANT STIFFNESS

Test results clearly show that near and beyond peak strength, cemented granular materials exhibit an increasing degradation of the initial secant stiffness due to micro-cracking. This effect is more evident after some unloading–reloading cycles, as shown in *Figure 12*.

A simple model of stiffness degradation appropriate for concrete is based on the assumption that it takes place only in the softening range and that the stiffness is proportional to the cohesion. That is, there is only one 'plastic degradation' variable δ such that:

$$\mathbf{D} = (1-\delta)\cdot\mathbf{D}_0 \tag{11}$$

where $\mathbf{D}_0$ is the elastic constitutive matrix prior to degradation and δ is governed by:

$$\mathrm{d}\delta = \frac{1-\delta}{c}\langle -\mathrm{d}c\rangle \tag{12}$$

the initial value of δ being zero. In any particular process then:

$$\delta = 1 - \frac{c}{c_{\text{peak}}}, \qquad \text{for } \mathrm{d}c < 0 \tag{13}$$

A more general model including elastic and plastic degradation effects has been recently developed by the authors and it is being currently tested[19,20].

MESH OBJECTIVITY

Objectivity of results with regard to the finite element mesh is obtained by introducing a constitutive equation depending on the element size and equalling the energy dissipated at each crack with that obtained from experimental tests. Here we have defined an uniaxial $\bar{\sigma}$–$\bar{\varepsilon}^p$ diagram obtained from a tension test such that the area under the diagram equals the specific fracture energy, g_f, (see *Figure 13*) with:

$$g_f = \frac{G_f}{h_f} \tag{14}$$

where G_f is the fracture energy and h_f is a typical dimension (characteristic length) of the influence zone where damage is localized. In the examples shown in the paper we have chosen:

$$h_f = \sqrt{A^e} \tag{15}$$

where A^e is the area of the element. A consistent way of obtaining the value of the 'characteristic length', h_f, has been recently proposed by Oliver[21] who introduces a 'smeared crack function' for averaging the discontinuous displacement field due to cracking over a single element. This allows one to obtain a simple expression for h_f in terms of the element dimensions and the direction of cracking within the element, which seems very adequate for objective numerical finite element analysis of localized cracking.

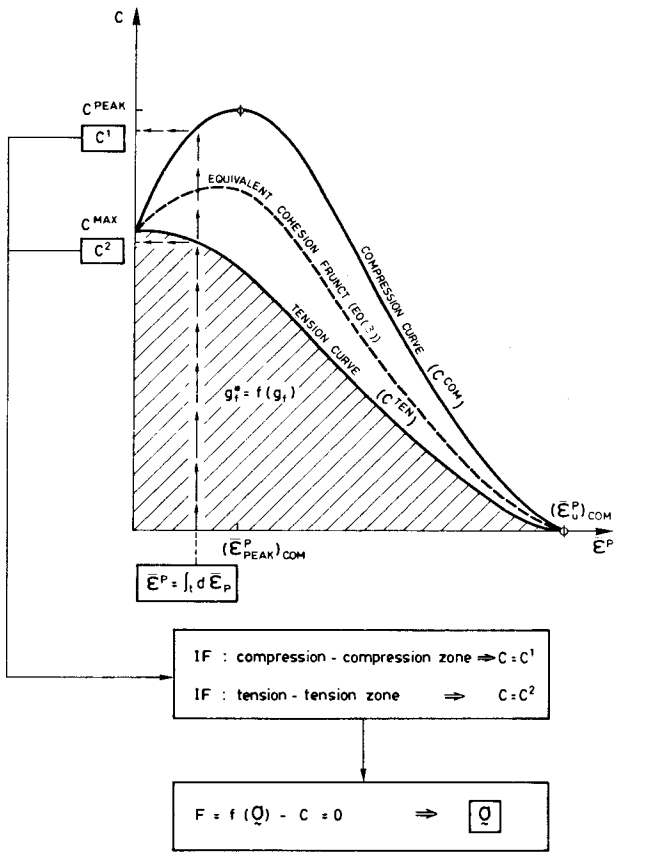

Figure 13 Cohesion curves for tension/compression behaviour, and specific fracture energy

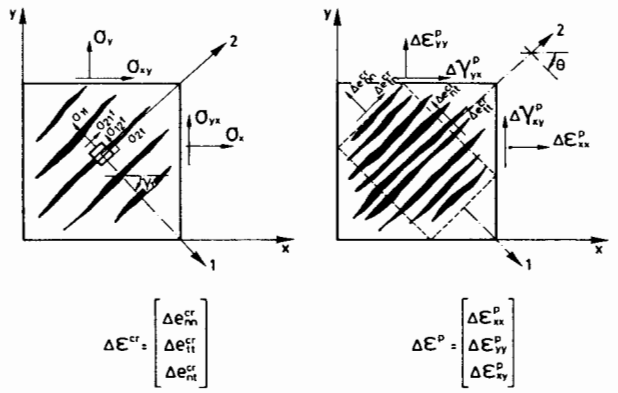

Figure 14 Direction of cracking

DETERMINATION OF CRACKS BY POSTPROCESSING THE NUMERICAL RESULTS

The amount and directions of cracking at a point in the model presented is obtained *a posteriori*, once convergence of the non-linear solution has been reached, as follows:

(a) Cracking initiates at a point when the effective plastic strain, $\bar{\varepsilon}^p$, is greater than zero. The direction of cracking is assumed to be orthogonal to that of the maximum principal strain at the point (see *Figure 14*).

(b) The increment of plastic strains along the directions of the crack, $\Delta\mathbf{e}^{cr}$, can be obtained as $\Delta\mathbf{e}^{cr}=\mathbf{T}\cdot\Delta\boldsymbol{\varepsilon}^p$, where $\Delta\boldsymbol{\varepsilon}^p$ is the vector of plastic strain increments expressed in global Cartesian axes and $\mathbf{T}$ is a transformation matrix given by:

$$\mathbf{T}=\begin{bmatrix} \cos^2\theta & \sin^2\theta & \dfrac{\sin 2\theta}{2} \\ \sin^2\theta & \cos^2\theta & -\dfrac{\sin 2\theta}{2} \\ -\sin 2\theta & \sin 2\theta & \cos 2\theta \end{bmatrix} \quad (16)$$

where θ is the angle which the direction of the maximum principal strain forms with the global x axis (see *Figure 14*).

Vector $\Delta\mathbf{e}^{cr}$ is used to accumulate the plastic strain dissipated along the crack local axes.

(c) The energy dissipated in the structure due to cracking in a load increment is obtained as:

$$\Delta W^p=\int_V \boldsymbol{\sigma}^T\cdot\Delta\boldsymbol{\varepsilon}^p\cdot dv \quad (17)$$

where V is the volume of the structure.

(d) The model also allows one to obtain the shear retention factor at a crack as $\beta=\tau/\tau^e$ where τ is the actual shear stress parallel to the direction of the crack and τ^e is the value of τ obtained from a linear elastic analysis.

Therefore, the elasto-plastic model proposed here allows the deduction of all the necessary information for fully defining the state of cracking in the structure. However, the fact that all this information is obtained *a posteriori* can be considered a clear advantage with respect to other discrete or smeared cracking models, which involve detailed transformations in each crack during the non-linear numerical solution stage.

EXAMPLES

Example I: 2-D analysis of a plain concrete cantilever

The cantilever of *Figure 15* has been analysed under displacement-controlled conditions using the three finite element meshes of 6, 24 and 96 standard isoparametric two-dimensional eight-node elements shown in the same Figure where all the relevant material data are also given.

Numerical results obtained for the load–displacement curve for the three meshes used have been plotted in *Figure 16a*. It is interesting to note the coincidence of results for the peak load for all meshes. *Figure 16b* shows the value of the dissipated energy, W^p, *versus* the end displacement. It is deduced from *Figure 16b* that the total energy converges towards the correct input value, thus showing the objectivity of results with respect to the mesh size.

In *Figure 16c* the change in stress in the most damaged integrating point is shown. Finally, in *Figure 17*, the localization of cracking for the three meshes used is clearly displayed. It is worth noting that the failure mechanism in the real test corresponds to a single crack.

Example II: Prestressed cantilevel beam

The beam shown in *Figure 18* has been subjected to a numerical test consisting of (a) prestressing in a direction parallel to the natural axis, and (b) subsequent transverse loading as shown in *Figure 18*. This corresponds to an experimental test numerically studied with some modifications by Rots *et al.*[4]. The numerical data for this example have been obtained from Reference 4.

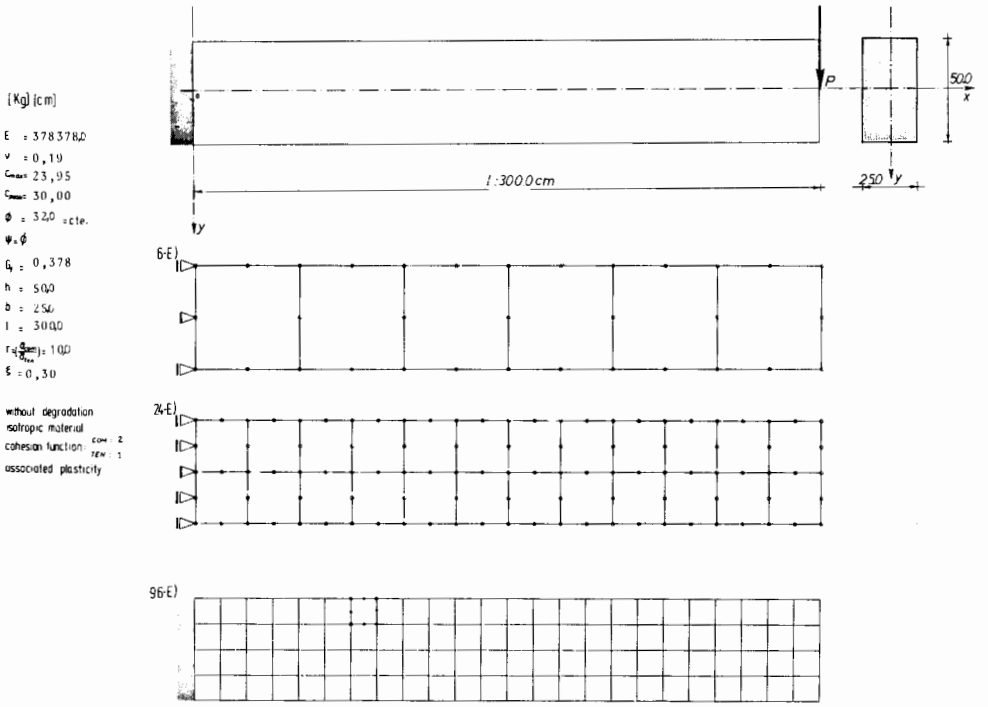

Figure 15 Cantilever beam, relevant material parameters, and finite element meshes

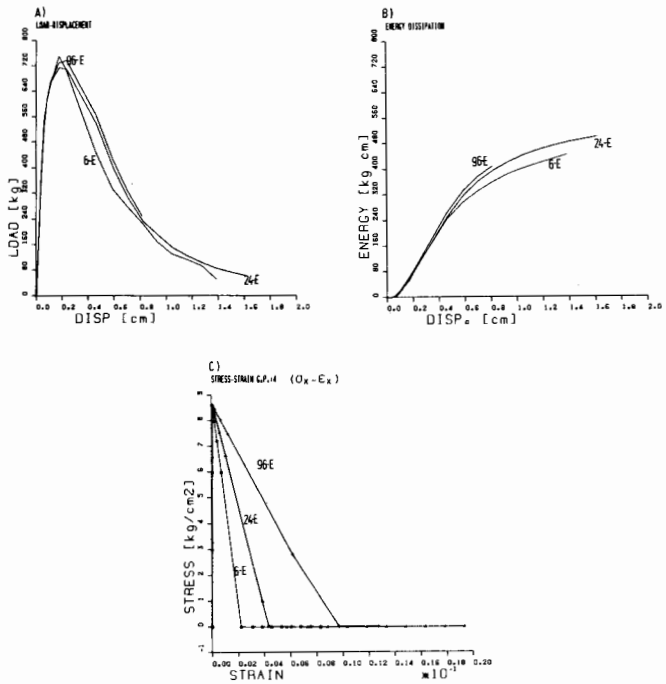

Figure 16 Cantilever beam: (a) load–displacement; (b) energy–dissipation; (c) stress–strain in the more damaged integrating point

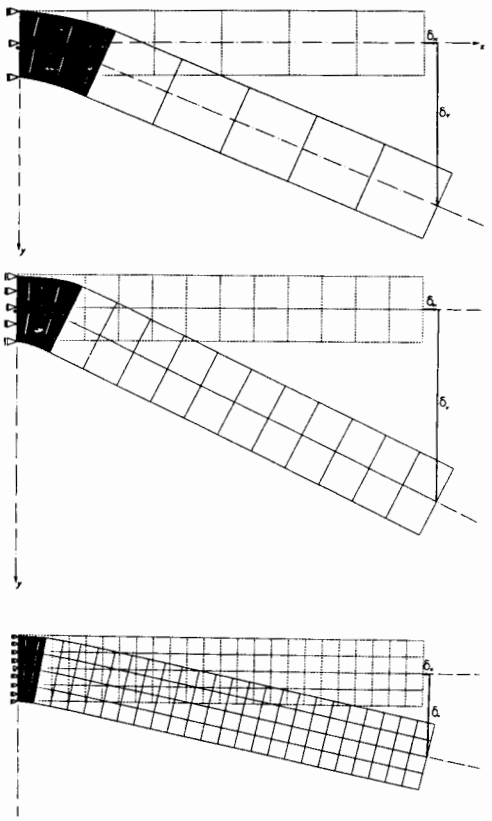

Figure 17 Cantilever beam, localization of cracking for the three meshes used

The material parameters and finite element mesh used are shown in *Figure 18*. Four node elements have been employed in the narrow band shown in *Figure 18*, whereas eight-node elements are used in the rest of the beam. 2×2 Gaussian quadrature has been used for all elements.

The load–displacement curve obtained is plotted in *Figure 19a*. Comparison of results obtained with those presented in Reference 4 is good. It can be

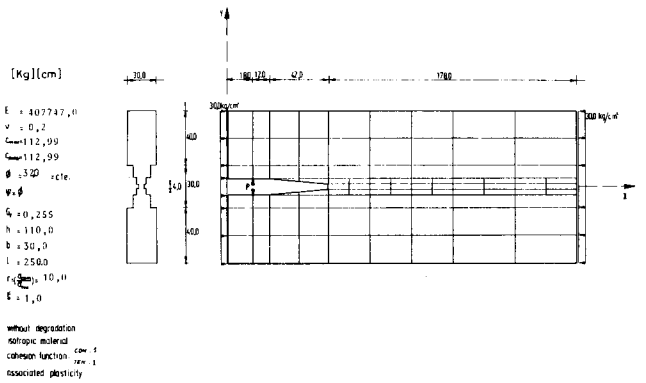

Figure 18 Prestressed beam relevant material parameters, and finite element meshes

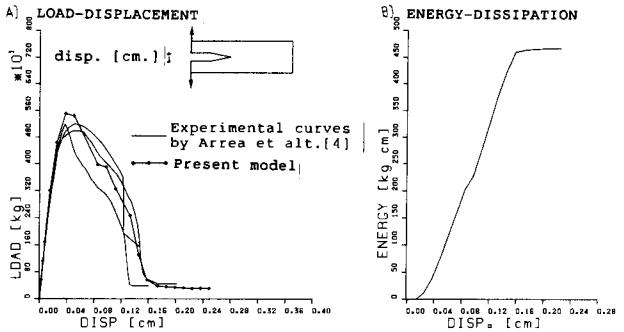

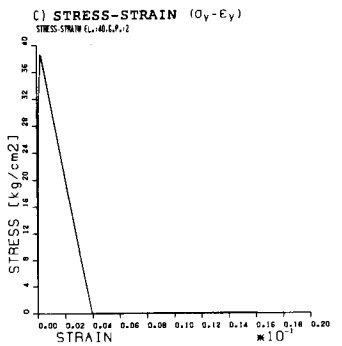

Figure 19 Prestressed beam: (a) load–displacement; (b) energy–dissipation; (c) stress–strain in the more damaged integrating point

seen that the applied load does not reach a zero value. This is due to the vertical component of the prestressing load, which opposes the opening of the two beam edges (see *Figure 19d*). The dissipated energy is shown in *Figure 19b*, where it can be seen that the solution stabilizes to the correct value. In *Figure 19c* the stress changes in the point under more severe damage is presented. Finally, *Figure 19d* clearly shows the localization of deformation. Again it is worth noting that the cracked elements simulate the effect of a single crack occurring in practice. Also note in *Figure 19d* the small transverse cracks due to local bending of the two beam edges.

Example III: Simple tension test of plain concrete specimen

The geometry of the specimen and material data is shown in *Figure 20*. Experimental results for this test were obtained by Peterson[22]. Two different meshes of 12 and 30 eight-node isoparametric elements were used in the analysis as shown in *Figure 20*. The specimen was analysed under displacement controlled conditions. Numerical results for the load–displacement curve are shown in *Figure 21a* and we can see a good coincidence of results for different meshes used in this example. The objectivity of the solution is evidenced in *Figure 21b* where the fracture energy obtained for different displacements has been plotted for the two meshes. It can be clearly seen that the two meshes yield the same total fracture energy. Finally, the distribution and localization of cracks is shown in *Figure 21c*.

CONCLUSIONS

An elasto-plastic model based on a modified Mohr–Coulomb yield surface for the non-linear analysis of concrete has been presented. The model

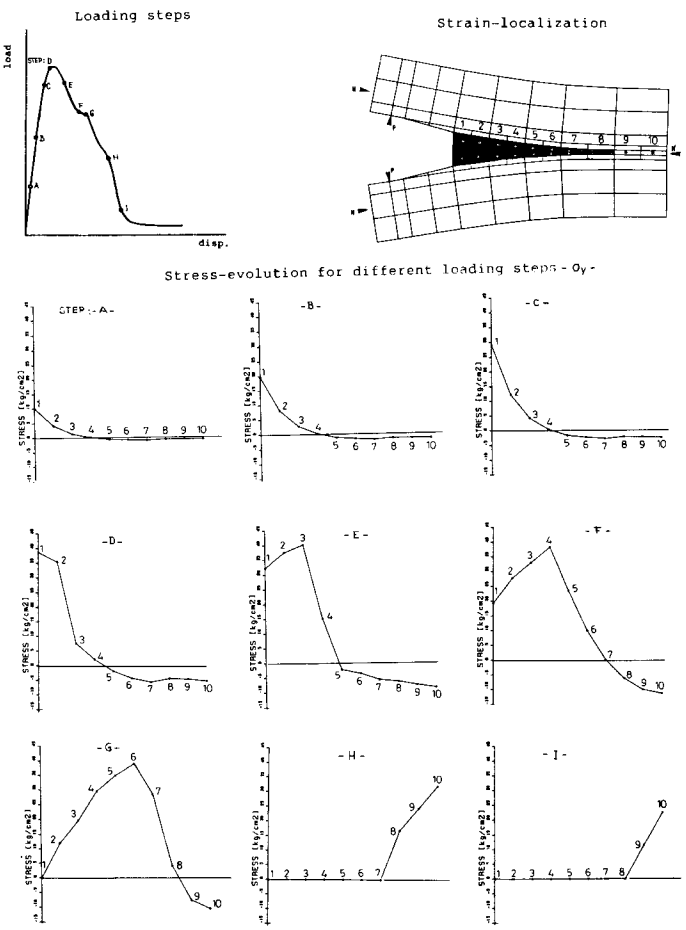

Figure 19d Prestressed beam: localization of cracking, and stress evolution

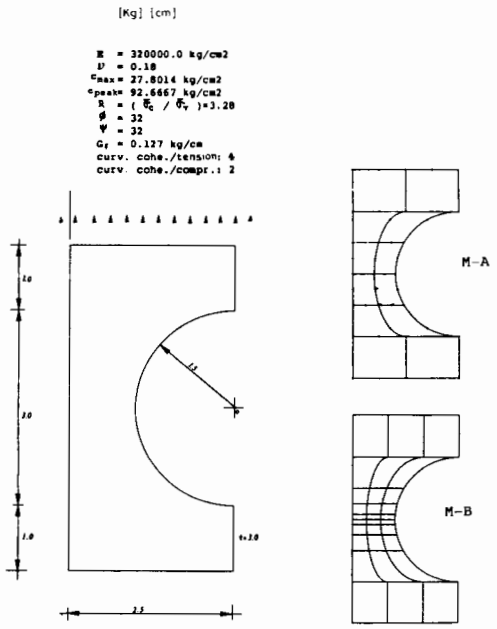

Figure 20 Simple tension test relevant material parameters, and finite element meshes

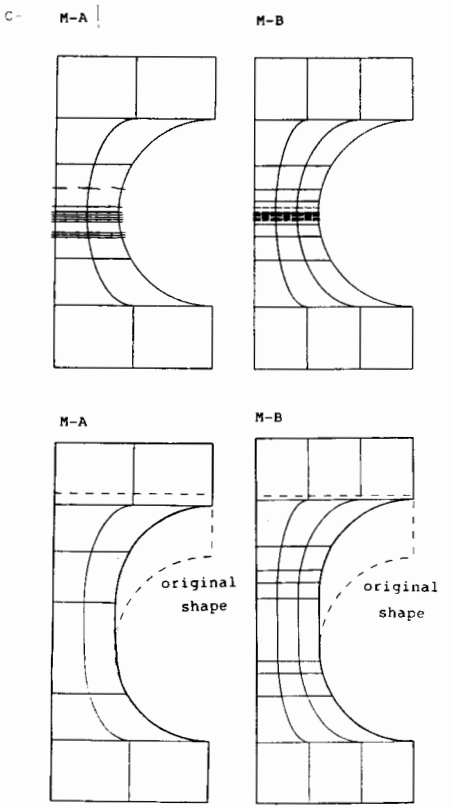

Figure 21b Simple tension test: (c) distribution and localization of cracking

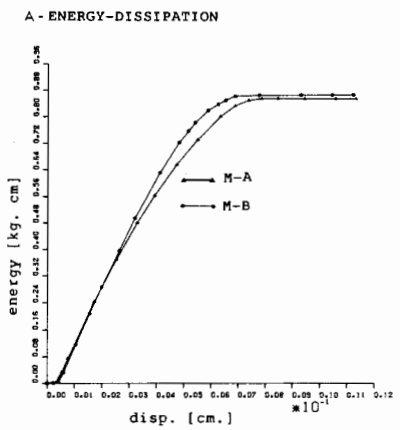

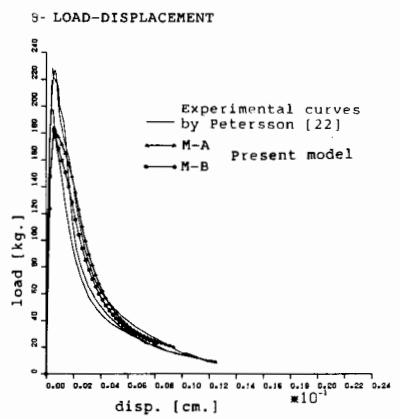

Figure 21a Simple tension test: (a) energy-dissipation; (b) load-displacement

seems adequate for predicting both non-linear tension (cracking) and compression behaviour of concrete by using the unified frame of plasticity theory. The directions and amount of cracking are obtained *a posteriori* by a simple postprocessing of numerical results. The examples analysed show that the model can be used for objectively reproducing localized behaviour, load–displacement history and distribution of cracking.

A generalization of the model to account for elastic and plastic degradation effects is currently investigated by the authors[19,20].

REFERENCES

1 Bazant, Z. and Oh, B. Crack band theory for fracture of concrete, *Mat. Construct.*, **16**, 155–177 (1983)
2 Glemberg, R. Dynamic analysis of concrete structures, *PhD Thesis*, Department of Structural Mechanics, Chalmers University of Technology, Goteborg, Sweden (1984)
3 De Borst, R. and Vermeer, P. Non-associated plasticity for soils, concrete and rock, *Heron*, **29** (3), 1–64 (1984)
4 Rots, J. G., Nauta, P., Kusters, G. and Blaauwendraad, J. Smeared crack approach and fracture localization in concrete, *Heron*, **30** (1985)
5 De Borst, R. Non-linear analysis of frictional material, *PhD Thesis*, Univ. of Delft, The Netherlands (1986)
6 Bazant, Z. Mechanics of distributed cracking, *Appl. Mech. Rev.*, **39**, 675–705 (1986)
7 Cedolin, D. Sull'applicabilità della meccanica della frattura al calcestruzzo, *Testimonianze e Note Scientifiche in Onore del*

Settantesimo Compleanno di Sandro dei Poli, Politecnico di Milano, Dipartimento di Ingegneria Strutturale, pp. 507–519 (1985)
8 Ronca, P. Simulazione numerica di prove a trazione per elementi bidimensionali in calcestruzzo, *Testimonianze e Note Scientifiche in Onore del Settantesimo Compleanno di Sandro dei Poli*, Politecnico di Milano, Dipartimento di Ingegneria Strutturale, pp. 507–519 (1985)
9 Mindess, S. Fracture toughness testing of cement and concrete, *Fracture Mechanics of Concrete: Material Characterization* (Eds. A. Carpinteri and A. Ingraffea), The Hague, pp. 67–110 (1984)
10 Bazant, Z. Instability, ductility and size effect in strain softening concrete, *J. Eng. Mech. Div., ASCE*, **102**, 331–344 (1976)
11 Ditommaso, A. Fracture mechanics of concrete, *Material Characterization and Testing, Evaluation of Concrete Fracture* (Eds. A. Carpinteri and A. Ingraffea), The Hague, pp. 31–76 (1984)
12 Creus, G. Instability, ductility and size effect in strain softening concrete. Discussion, in *J. Eng. Mech. Div., ASCE Proc. Paper 12042* (1977)
13 Chen, A. C. and Chen, W. Constitutive relations for concrete, *J. Eng. Mech. Div., ASCE*, **101**, 465–481 (1975)
14 Oñate, E., Oller, S., Oliver, J. and Lubliner, J. A constitutive model for cracking of concrete based on the incremental theory of plasticity, *Int. Conf. Comput. Plasticity* (Eds. D. R. J. Owen, E. Hinton and E. Oñate), Pineridge Press, Swansea (1987)
15 Oñate, E., Oller, S., Oliver, J. and Lubliner, J. A fully elastoplastic model for non-linear analysis of concrete, *Int. Conf. Num. Methods in Engng. Theory and Applications, NUMETA* (Eds. G. N. Pande and J. Middleton), Martinus Nijhoff (1987)
16 Hinton, E. and Owen, D. R. J. *Finite Elements in Plasticity*, Pineridge Press, Swansea (1980)
17 Rowe, P. W. Theoretical meaning and observed values of deformation parameters for soil, *Proc. Rascoe Mem. Symp. on Stress Strain Behaviour of Soils, Cambridge*, pp. 143–194 (1972)
18 Dougill, J. W. Constitutive relations for concrete and rock: Applications and extensions of elasticity and plasticity theory, *Mechanics of Geomaterials* (Ed. Z. Bazant), Ch. 3, pp. 21–46 (1985)
19 Lubliner, J., Oller, S., Oliver, J. and Oñate, E. A plastic damage model for non-linear analysis of concrete, *Internal Report*, ETS Ing. Caminos, Univ. Politécnica de Catalunya, Barcelona (1988)
20 Oller, S. Un modelo de daño plástico para materiales friccionales, *PhD Thesis*, ETS Ing. Caminos, Univ. Politécnica de Catalunya, Barcelona (1988)
21 Oliver, J. On smeared numerical models for the analysis of localized cracking in concrete, *Int. J. Num. Meth. Eng.*, in press (1989)
22 Peterson, P. E. Crack growth and development of fracture zones in plain concrete and similar materials, *Report TVBM-1006*, Division of Building Materials, Lund Institute of Technology.

View publication stats